

Tomographic Image Reconstruction from Incomplete View Data by Convex Projections and Direct Fourier Inversion

M. IBRAHIM SEZAN AND HENRY STARK

Abstract—We consider the problem of reconstructing CAT imagery by the direct Fourier method (DFM) when not all view data are available. To restore the missing information we use the method of projections onto convex sets (POCS). POCS is a recursive image restoration technique that finds a solution consistent with the measured data and *a priori* known constraints in both the space and Fourier domain. Because DFM reconstruction is a frequency-domain technique it is ideally matched to POCS restoration when, for one reason or another, we are forced to generate an image from a less than complete set of view data.

We design and apply an algorithm (PRDF) which interpolates/extrapolates the missing Fourier domain information by POCS and reconstructs an image by DFM. A simulated human thorax cross section is restored and reconstructed. The restorations using POCS are compared with the Gerchberg-Papoulis extrapolation method and shown to be superior. Applications of PRDF to other types of medical imaging modalities are discussed.

I. INTRODUCTION

IN this paper we combine the direct Fourier method (DFM) of reconstructing from projections with an iterative restoration algorithm called projections onto convex sets¹ (POCS) to reconstruct good quality imagery from incomplete projection data. The method of POCS was discussed in two recent papers in this TRANSACTIONS [1], [2] in connection with image restoration when only partial frequency or space domain data were available to reconstruct an arbitrary image. Lent and Tuy [3] appear to have been the first to restore an image using the POCS algorithm.² Tuy [4] has used POCS to restore missing projection data in connection with reconstruction, via filtered convolution back-projection (FCBP). Although they have demonstrated impressive results, their algorithm requires the time-consuming artifice of generating projection data at each iteration that is consistent with *a priori* constraints.³ Since constraints are generally applied to the image or its spectrum (but not its projections), we were motivated to study the restoration from the incomplete projections problem from a different viewpoint.

It is important for the reader to distinguish between the

Manuscript received December 1, 1983. This work was supported by the National Science Foundation under Grant ECS-81-11264.

M. I. Sezan was with Rensselaer Polytechnic Institute, Department of Electrical, Computer, and Systems Engineering, Troy, NY 12181. He is now with Eastman Kodak Research Labs, Rochester, NY 14650.

H. Stark is with Rensselaer Polytechnic Institute, Department of Electrical, Computer, and Systems Engineering, Troy, NY 12181.

¹Projection onto convex sets refers to *mathematical* projections while projections in CAT refer to line integrals. It should be clear from context which projection is meant.

²Others who have used similar methods with good success are Tam and Perez-Mendes [24].

³An algorithm closely related to Tuy's is discussed by Medoff *et al.* [22].

processes of reconstruction and restoration. As commonly used, by reconstruction we mean the activity of generating an image (analytically or otherwise) from an essentially complete set of data which are not in image format to begin with, e.g., the way a TV image is reconstructed from an electrical signal, or the way an image is reconstructed from a hologram.

In contrast, by restoration we mean the activity of improving the quality of an image, or the data from which the image is reconstructed by combining *a priori* known properties of the image with measured data. Restoration generally implies an incomplete data set, e.g., incomplete view data in tomography, a low-pass blurred image in photography, or loss of phase, as in X-ray diffraction.

Although reconstruction and restoration may seem like dissimilar activities they have in fact, fundamentally, much more in common than at first perceived. We shall not pursue this point much further except for pointing out that in restoration the existing data together with the *a priori* constraints often suffice to uniquely determine an image. Then, one can argue that all the data are there and the problem is how to convert them to image format. But is this not essentially the definition of reconstruction? Despite this obvious problem with the definitions, we shall restrict our definitions in this paper to the common usage mentioned earlier.

It might be well to consider why in computer-aided tomography (CAT)—a process which is highly controllable—one should be forced to work with incomplete view data. In X-ray diffraction, optical astronomy and indeed, many other scientific imaging type measurements, one *cannot* obtain all the data (directly at least) needed to obtain the desired image. For example, in X-ray diffraction, the phase that furnishes depth information is lost, while in optical astronomy both atmospheric turbulence and finite-aperture optics limit the resolving power of the instrument. In CAT, there are several reasons why an incomplete view data situation might prevail. In medical CAT, there may be insufficient time for 360 degree data acquisition of time varying anatomical situations. In industrial applications, e.g., inspection, incomplete view data can result when obstructions prevent 360 degree viewing, or when imaging a moving part or a time varying event.

Since image reconstruction from incomplete view data is not merely of academic interest, one next has to deal with the choice of restoration/reconstruction. Why DFM/POCS? With regard to the method of restoration, POCS offers two noteworthy advantages: 1) it enables any number of *a priori* convex-type constraints⁴ to be incorporated in the algorithm; and

⁴Defined in Section II.

2) it guarantees convergence: weak in general, strong in practice. Having chosen POCS as the restoration algorithm, the logical reconstruction method is the direct Fourier method (DFM). Not only is DFM as fast as a reconstruction algorithm, but because it involves transformations between space and Fourier domains, it enables space-domain and Fourier-domain constraints to be applied in their respective spaces directly. Finally, because exact interpolation formulas exist—which can be realized in practice to a high degree of accuracy—a DFM-reconstructed image can be made the same quality as by the method of filtered convolution back-projection (FCBP).

The organization of this paper is as follows. In Sections II and III, we briefly review the POCS and DFM algorithms. In Section IV, we describe the PRDF algorithm which combines POCS and DFM into a single restoration/reconstruction module. In Sections V and VI, we describe the experimental data and the results of applying PRDF. In Section VII, we briefly discuss the potential application of PRDF to imaging problems in NMR and ultrasound tomography. And, in Section VIII, we summarize the paper.

II. REVIEW OF THE METHOD OF PROJECTIONS ONTO CONVEX SETS (POCS)

The method of POCS has been discussed in some detail in [1] and [2]. Strictly for the reader's convenience, we review here only the central idea of POCS and give the projection operators (without derivation) of use in CAT.

The image to be restored, $f(x, y)$ is assumed to be an element of the Hilbert space \mathbb{H} of square-integrable functions.

The basic idea of POCS is as follows: every known property of the unknown $f \in \mathbb{H}$ will restrict f to lie in a closed convex set \mathcal{C}_i in \mathbb{H} . Thus, for m known properties there are m closed convex sets \mathcal{C}_i , $i = 1, 2, \dots, m$ and $f \in \mathcal{C}_o \triangleq \cap_{i=1}^m \mathcal{C}_i$. Then, the problem is to find a point of \mathcal{C}_o given the sets \mathcal{C}_i and projection operators P_i projecting onto \mathcal{C}_i , $i = 1, 2, \dots, m$. The convergence properties of the sequence $\{f_k\}$ generated by the recursion relation

$$f_{k+1} = P_m P_{m-1} \cdots P_1 f_k; \quad k = 0, 1, \dots \quad (1)$$

or more generally by

$$f_{k+1} = T_m T_{m-1} \cdots T_1 f_k; \quad k = 0, 1, \dots \quad (2)$$

with $T_i \triangleq I + \lambda_i(P_i - I)$, $0 < \lambda_i < 2$, are based on fundamental theorems given by Opial [6] and Gubin *et al.* [7]. The λ_i 's $i = 1, \dots, m$ are relaxation parameters, and can be used to accelerate the rate of convergence of the algorithm. However, the λ 's that are effective in the absence of noise will often be ineffective when noise is present [5]. Thus, a single set of λ 's is not effective at all signal-to-noise ratios. The following sets and their associated projection operators are among the ones used in [2] and [5] and they will be used here.

1) \mathcal{C}_1 : The set of all functions in \mathbb{H} that vanish outside a prescribed region $\delta \subset \Omega$. Given an arbitrary f in \mathbb{H} its projection onto \mathcal{C}_1 is realized by

$$P_1 f = \begin{cases} f, & (x, y) \in \delta \\ 0, & (x, y) \notin \delta. \end{cases} \quad (3)$$

2) \mathcal{C}_2 : The set of all functions in \mathbb{H} whose Fourier transforms assume a prescribed value G over a closed region \mathfrak{L} in the $u-v$ Fourier plane. The projection of an arbitrary f in \mathbb{H} is realized by

$$P_2 f \leftrightarrow \begin{cases} G(u, v), & (u, v) \in \mathfrak{L} \\ F(u, v), & (u, v) \notin \mathfrak{L} \end{cases} \quad (4)$$

where $F(u, v) = \mathcal{F}[f(x, y)]$ and \mathcal{F} is the Fourier transform operator. In the case of incomplete view data, $G(u, v)$ is known in a data cone with a subtended angle of less than 180 degrees.

3) \mathcal{C}_3 : The set of all real valued nonnegative functions in \mathbb{H} that satisfy the energy constraint

$$\iint_{\Omega} |f(x, y)|^2 dx dy \leq E \triangleq \rho^2. \quad (5)$$

To describe the projection onto \mathcal{C}_3 , we write $f \triangleq f_1 + jf_2$ where $f_1 = \text{Re}(f)$ and $f_2 = \text{Im}(f)$ and let f_1^+ be the rectified portion of f_1 , i.e., $f_1^+ = f_1$ when $f_1 > 0$ and $f_1^+ = 0$ when $f_1 \leq 0$. Then the projection of an arbitrary $f \in \mathbb{H}$ onto \mathcal{C}_3 is realized by

$$P_3 f = \begin{cases} 0, & f_1 < 0 \\ f_1^+, & E_1^+ \leq E \\ \sqrt{\frac{E}{E_1^+}} f_1^+, & E_1^+ > E \end{cases} \quad (6)$$

where E_1^+ is the energy in f_1^+ , i.e.,

$$E_1^+ \triangleq \iint_{\Omega} (f_1^+)^2 dx dy. \quad (7)$$

4) \mathcal{C}_4 : The set of all real valued f 's in \mathbb{H} whose amplitudes must lie in a prescribed closed interval $[a, b]$; $a \geq 0$, $b > 0$, $a < b$. The projection onto \mathcal{C}_4 is realized by the following rule

$$P_4 f = \begin{cases} a, & f(x, y) < a \\ f(x, y), & a \leq f(x, y) \leq b \\ b, & f(x, y) > b. \end{cases} \quad (8)$$

Operators P_1 , P_2 , P_3 , and P_4 were used in (1) and (2) in restoring an image from its noiseless partial frequency spectrum [2]. They were also used together with a noise smoothing operator to restore images from noisy partial frequency spectrum [5]. In all cases the method of POCS outperformed the Gerchberg-Papoulis (G-P) algorithm⁵ [8].

III. REVIEW OF THE DIRECT FOURIER METHOD (DFM) OF RECONSTRUCTION FROM PROJECTIONS

The DFM is based on the central slice projection theorem [9]. Let $\mu(x, y)$ represent a function whose image is desired (e.g., in CAT, $\mu(x, y)$ is the X-ray absorptivity). Let $\mu_{\phi}(\hat{x}, \hat{y})$ represent the same distribution in a coordinate system $\hat{x}-\hat{y}$

⁵The G-P algorithm also involves projections onto convex sets (actually linear subspaces), but generally ignores most *a priori* known constraints except space-limitedness and band-limitedness.

rotated from x - y by an angle ϕ . The projection data at view angle ϕ is defined as

$$p_\phi(\hat{x}) \triangleq \int_L \mu_\phi(\hat{x}, \hat{y}) d\hat{y} \quad (9)$$

where L is the beam path. The central slice projection theorem states that

$$P_\phi(\rho) = M(\rho, \phi), \quad \rho \geq 0 \quad 0 < \phi \leq 2\pi \quad (10a)$$

where

$$P_\phi(\rho) = \int_{-\infty}^{\infty} p_\phi(\hat{x}) e^{-i2\pi\rho\hat{x}} d\hat{x} \quad (10b)$$

and $M(\rho, \phi)$ denotes the 2-D Fourier transform of the cross-section distribution $\mu(x, y)$ in polar coordinates. In practice $p_\phi(\hat{x})$ is the data actually obtained at the location of detectors $\{\hat{x}_j\}$. In place of (10b) the discrete Fourier transform is used to obtain $P_\phi(\rho)$ at the discrete set of spatial frequencies $\{\rho_n\}$. Since the view angles are also a discrete set $M(\rho, \phi)$ is known at points on a polar grid $\{\rho_n, \phi_k\}$, $n = 1, 2, \dots, N$; $k = 1, 2, \dots, 2K + 2$ where N is the number of detectors, K is the highest harmonic in the angularly band-limited image and $\phi_k = (2\pi/2K + 2)k$.

At this point, direct Fourier methods require interpolating $M(\rho_n, \phi_k)$ to $M_c(u_l, v_m)$ where $M_c(\cdot)$ is the Fourier transform of $\mu(x, y)$ on a Cartesian raster. The interpolation from a polar to Cartesian raster is required in order to use the FFT routine. However, inexact interpolation is a major source of error in reconstruction by direct Fourier methods even when the interpolation errors are not large (Lewitt [10] discusses this point in some detail). Attempts at implementing DFM using nearest neighbor and linear interpolation were done by Mersereau and Oppenheim [11]. Interpolation of temporal signals (that contain spatial frequency information) for NMR reconstruction is discussed by Cho *et al.* in [12].

Recently an exact interpolation method was discussed [9], [13], [14] which, in direct comparison and under practical constraints, produced images equal or superior in quality to convolution back-projection methods. The method is based on the *exact polar sampling theorem*

$$M(\rho, \phi) = \sum_{n=-\infty}^{\infty} \sum_{k=0}^{\infty} M\left(\frac{n}{2A}, \frac{\pi k}{K+1}\right) \cdot \text{sinc}\left[2A\left(\rho - \frac{n}{2A}\right)\right] \sigma\left(\phi - \frac{\pi k}{K+1}\right) \quad (11a)$$

where $2A$ is the diameter that bounds the object in space, K is the highest angular frequency in the periodic function $M(\rho, \phi)$, and $\sigma(\phi)$ is an azimuthal interpolating function given by

$$\sigma(\phi) \triangleq \frac{\sin[(K+1)\phi]}{(2K+2)\sin[(1/2)\phi]}. \quad (11b)$$

The proof of (11a) is given in [13]. Its use is as follows: to compute $M_c(u_l, v_m)$, (11a) is used with

$$\rho_{lm} \triangleq \sqrt{u_l^2 + v_m^2} \quad (12)$$

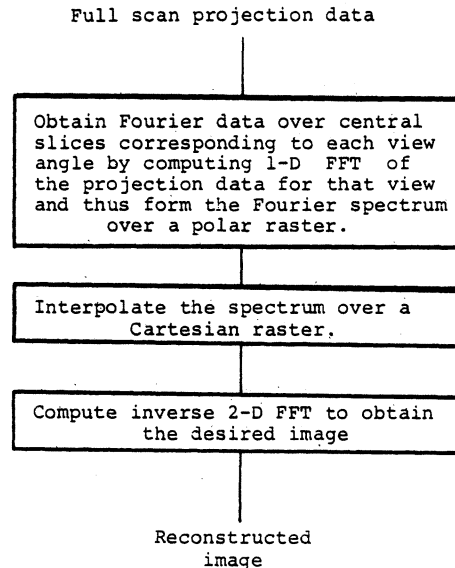


Fig. 1. Direct Fourier method (DFM).

$$\phi_{lm} \triangleq \cos^{-1}\left(\frac{u_l}{\rho_{lm}}\right). \quad (13)$$

Thus, the set $\{u_l, v_m\}$ can be computed directly from the set $\{\rho_n, \phi_k\}$. In practice a truncated interpolation involving a finite number of cardinal functions is used. Thus, (11a) is replaced by

$$\hat{M}(\rho, \phi) = \sum_{n=n_p-L_\rho}^{n_p+L_\rho} \sum_{k=k_\phi-L_\phi}^{k_\phi+L_\phi} M\left(\frac{n}{2A}, \frac{\pi k}{K+1}\right) \cdot \text{sinc}\left(2A\left(\rho - \frac{n}{2A}\right)\right) \sigma\left(\phi - \frac{\pi k}{K+1}\right) \quad (14)$$

where $[2A\rho] \triangleq n_p$ and $[(K+1)\phi/\pi] \triangleq k_\phi$,⁶ are the nearest neighbors to the point about which the expansion is done. In practice, image quality is improved when the truncation is tapered. The taper normally used is the Cartesian product of two identical one-dimensional triangular windows, $\omega(n)$, of the form

$$\omega(n) = \max(1 - |n|/M, 0); \quad n = 0, \pm 1, \pm 2, \dots \quad (15)$$

$M = \infty$ is the abrupt truncation case. If $L_\rho = L_\phi = 0$, the above practical approximation reduces to nearest neighbor approximation. In this paper, we use (14), i.e., exact interpolation with truncation and tapering ($M = 5$).

After interpolating the 2-D Fourier spectrum from a polar to a Cartesian raster, a 2-D inverse FFT is computed to obtain the desired image. The direct Fourier method is illustrated in Fig. 1.

IV. PRDF ALGORITHM

If projection data are available over a limited angular range, then the image Fourier transform $M(\rho, \phi)$ can be interpolated over a Cartesian grid within this angular range (the data cone). The pixels remaining outside this angular range are set to zero as a first approximation. The missing frequency information is

⁶The operation indicated by the brackets indicates the closest integer to the value within the brackets, i.e., rounding.

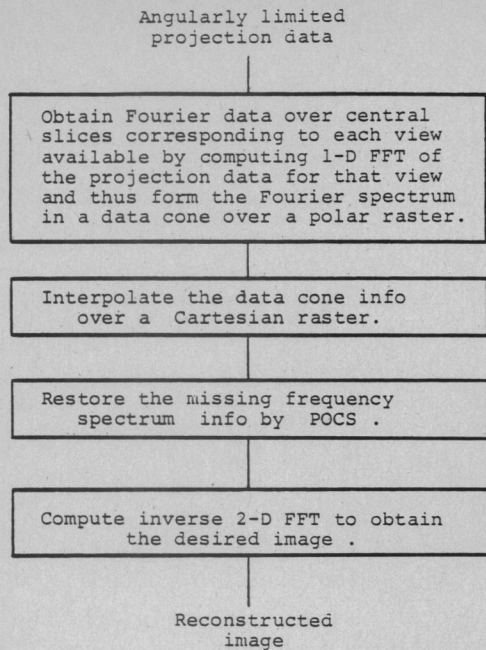


Fig. 2. PRDF algorithm for reconstructing from angularly limited view (projection) data.

then restored by POCS and the desired image is obtained by inverse transforming. The complete algorithm is called PRDF and it is illustrated in Fig. 2.

V. RECONSTRUCTING A THORAX PHANTOM FROM ANGULARLY LIMITED X-RAY PROJECTION DATA

The 128×128 pixels thorax phantom⁷ is shown in Fig. 3. The stimulated parallel beam projection data assume an X-ray energy of 70 keV, 128 detectors which are spaced apart by 0.3 cm and 360 views over 360 degrees. The interpolated transform with $L_\rho = 3$, $L_\phi = 1$, i.e., 21 interpolation points and resulting reconstruction from complete view data is shown in Fig. 4. The 11 percent reconstruction error⁸ between the reconstructed image and the original is due to 1) inadequate sampling of the projection data, 2) inadequate sampling in radial frequency, and 3) insufficient number of views. Since the object is of finite support the projection data at each view will also have finite support. Hence instead of obtaining $P_\phi(k/2A)$ one obtains a periodic extension

$$\hat{P}_\phi(k/2A) = \sum_{n=-\infty}^{\infty} P_\phi((k+nN)/2A) \quad k = 1, 2, \dots, N \quad (16)$$

in which the $n = 0$ term cannot be isolated without containing contamination from the $n \neq 0$ higher orders. However, this unavoidable effect can be reduced by choosing N (number of detectors) large enough. In practical situations the finite width of the X-ray beam produces smoothed projection data which is somewhat equivalent to low-pass filtering the projection data. Hence, in practice the effect of aliasing artifacts can

⁷The thorax phantom is widely used in the literature. It was designed by Herman and Lakshminarayanan.

⁸Percent error $\triangleq \|f_{\text{rec}} - f_{\text{true}}\|/\|f_{\text{true}}\| \cdot 100$.

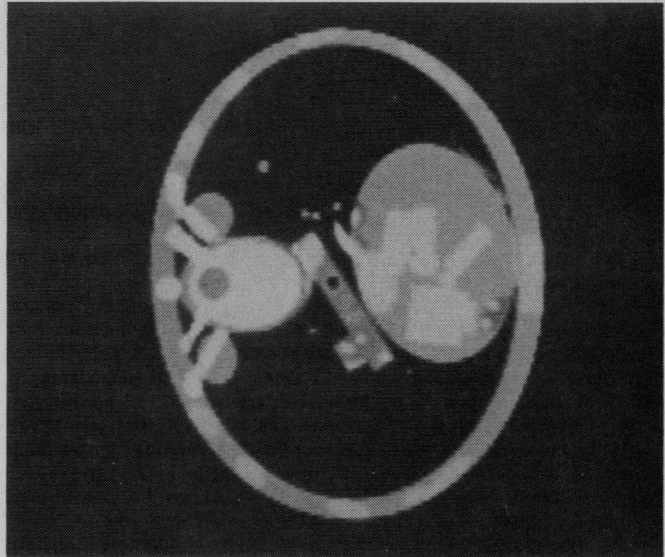


Fig. 3. Thorax phantom (through eighth vertebra).

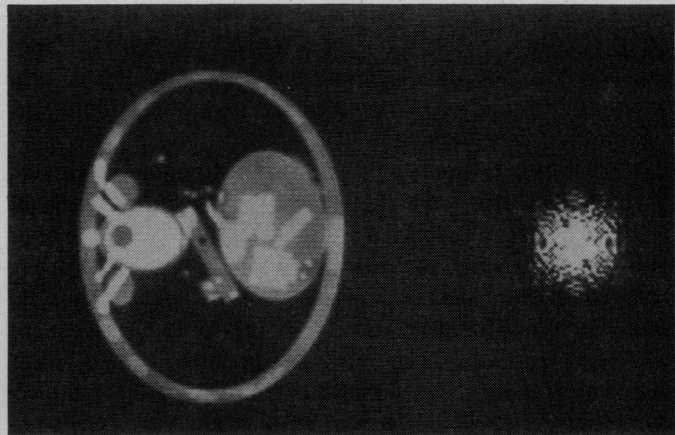


Fig. 4. DFM reconstruction and interpolated spectrum ($L_\rho = 3, L_\phi = 1$).

be made tolerably small. The other two effects are discussed at length in [9].

Reconstruction by PRDF from angularly limited projection data is attempted for the following three cases: projection data is limited to the view range of 1) $[-80^\circ, 80^\circ]$, 2) $[-67^\circ, 67^\circ]$, 3) $[-45^\circ, 45^\circ]$. The formula of (14) with $L_\rho = 3, L_\phi = 1$ is used to interpolate $\hat{M}(\rho, \phi)$ from polar to Cartesian points. The Fourier transform for full view data and the above three cases is shown after interpolation in Fig. 5.

VI. RESULTS

The basis for comparing results was the percent error e_k at the k th iteration defined by

$$e_k \triangleq 100 \cdot \frac{\|f - f_k\|}{\|f\|} \quad (17)$$

where $f \triangleq f(x, y)$ is the full scan (360 degrees) reconstructed image. While e_k is a standard measure for evaluating the efficacy of an image restoration algorithm, its relationship to subjective or clinical evaluation has not been established.

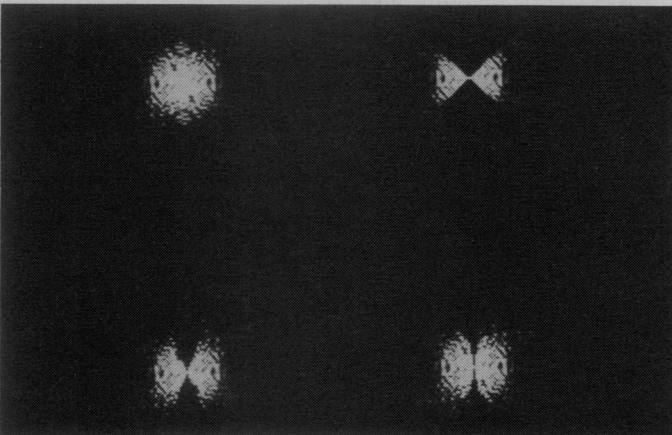


Fig. 5. Interpolated frequency spectrum. Clockwise from upper left: full view projection data, view limited to $[-45^\circ, 45^\circ]$, view limited to $[-80^\circ, 80^\circ]$, view limited to $[-67^\circ, 67^\circ]$.

TABLE I
SUMMARY OF *A Priori* ASSUMED CONSTRAINTS

<i>a priori</i> constraints	Actual
(1) Image support confined to rectangular region of length 124 pixels and width 103 pixels.	(1) Image support is elliptical (Figure 3).
(2) Gray levels f satisfy $0 \leq f \leq 0.4$	(2) Gray levels f satisfy $0 \leq f \leq 0.38$
(3) Energy over 128×128 square pixel field cannot exceed $\rho^2 = 284.000$	(3) Energy over 128×128 square pixel field is 282.74

TABLE II
SUMMARY OF SIGNIFICANT RESULTS

Available View Range	Algorithm			Percent Error	
	Name	Description	Relaxation Parameters	e_0 (zero-order solution)	e_{30}
$[-45^\circ, 45^\circ]$	GP	$P_2 P_1 f_k = f_{k+1}$	$\lambda_1 = \lambda_2 = 1.0$	52.419	47.511
	UNIRELAXL	$P_4 P_2 P_3 P_1 f_k = f_{k+1}$	$\lambda_1 = \lambda_2 = 1.0$ $\lambda_3 = \lambda_4 = 1.0$		42.057
$[-67^\circ, 67^\circ]$	GP	$P_2 P_1 f_k = f_{k+1}$	$\lambda_1 = \lambda_2 = 1.0$	45.000	22.203
	UNIRELAX	$P_2 P_3 P_1 f_k = f_{k+1}$	$\lambda_1 = \lambda_2 = \lambda_3 = 1.0$		17.837
$[-80^\circ, 80^\circ]$	RELAX	$T_2 T_3 T_1 f_k = f_{k+1}$	$\lambda_1 = \lambda_2 = \lambda_3 = 1.9995$ $\lambda_2 = 1.0$	41.361	16.184
	GP	$P_2 P_1 f_k = f_{k+1}$	$\lambda_1 = \lambda_2 = 1.0$		15.485
	UNIRELAX	$P_2 P_3 P_1 f_k = f_{k+1}$	$\lambda_1 = \lambda_2 = \lambda_3 = 1.0$		12.100
	RELAX	$T_2 T_3 T_1 f_k = f_{k+1}$	$\lambda_1 = \lambda_3 = 1.9995$ $\lambda_2 = 1.0$		9.352

A summary of the *a priori* known facts and assumptions made about the image are given in Table I. Table II furnishes a summary of the experimental results. The first (leftmost) column of Table II gives the angular field of view over which data are available; in the second column is the name of the restoration algorithm; in the third and fourth columns are the recursion relations and the associated values of the relaxation

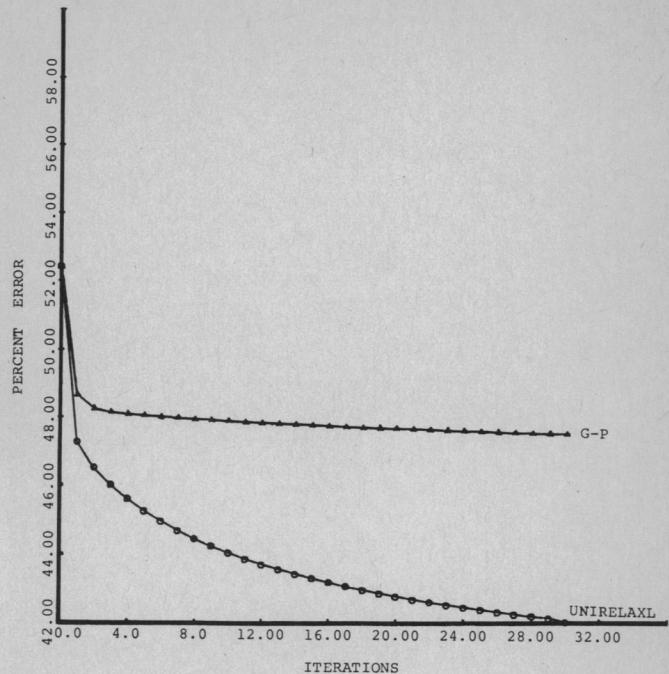


Fig. 6. Performance comparison of G-P, and UNIRELAXL in reconstructing from projection data available over $[-45^\circ, 45^\circ]$.

parameters, respectively; the next column is the error between the full scan image and the image immediately reconstructed from the limited view data (the so-called zero-order or "naive" solution); and the last column is the error at the 30th iteration for the three cases of angularly limited projection (view) data.

A. Results for When Projection Data Are Limited to $[-45^\circ, 45^\circ]$

In this case the reconstructed image at the end of 30 iterations is of low visual quality for all algorithms. Still the DFM reconstruction using UNIRELAXL (i.e., level constraints applied) restoration outperforms the DFM reconstruction using G-P restoration. The error performance of the reconstructions are compared in Fig. 6.

B. Results for When Projection Data Are Limited to $[-67^\circ, 67^\circ]$

In this case the three different restoration algorithms G-P, UNIRELAX, and RELAX are separately combined with DFM reconstruction. The naive solution, which is merely inverse Fourier transforming the polar to Cartesian interpolated spectrum having zeros for the entries corresponding to unavailable angular region (Fig. 5) results in an error of 45 percent. In Fig. 7 the naive solution is compared to reconstructions using G-P, UNIRELAX, and RELAX restorations. The error performance of these three reconstructions are compared in Fig. 8. With the RELAX restoration an error less than 17 percent is reached at the end of 30 iterations and the resulting reconstruction has fairly good visual quality (see Fig. 7). As can be seen from Figs. 7 and 8, PRDF reconstruction incorporating UNIRELAX and RELAX restoration outperforms the reconstruction based on G-P restoration.

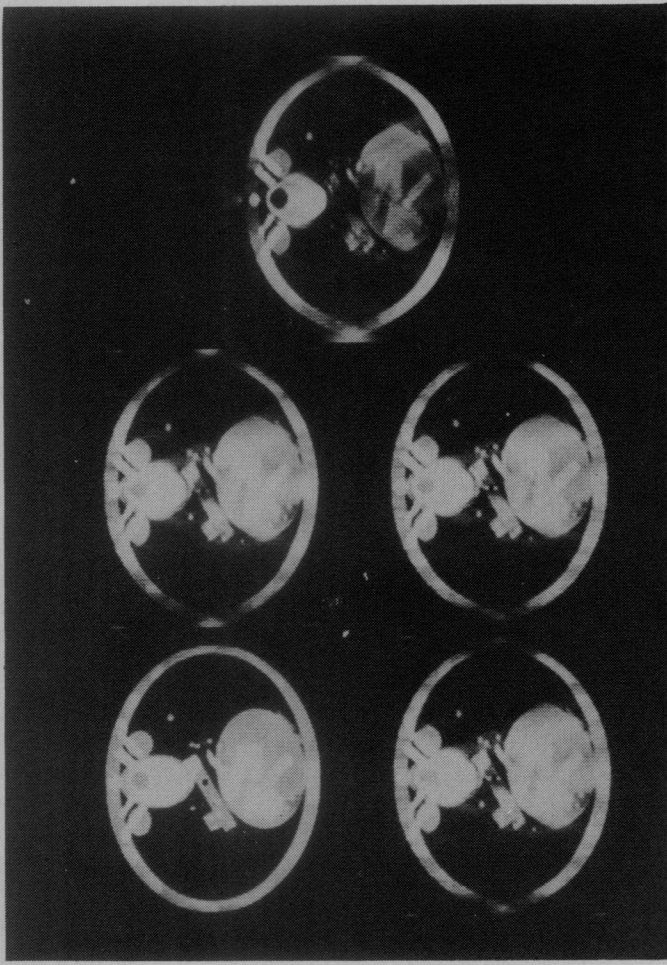


Fig. 7. Reconstructions when projection data are limited to $[-67^\circ, 67^\circ]$. Top: naive reconstruction; then clockwise from upper left: G-P, RELAX, UNIRELAX, and full view data reconstruction.

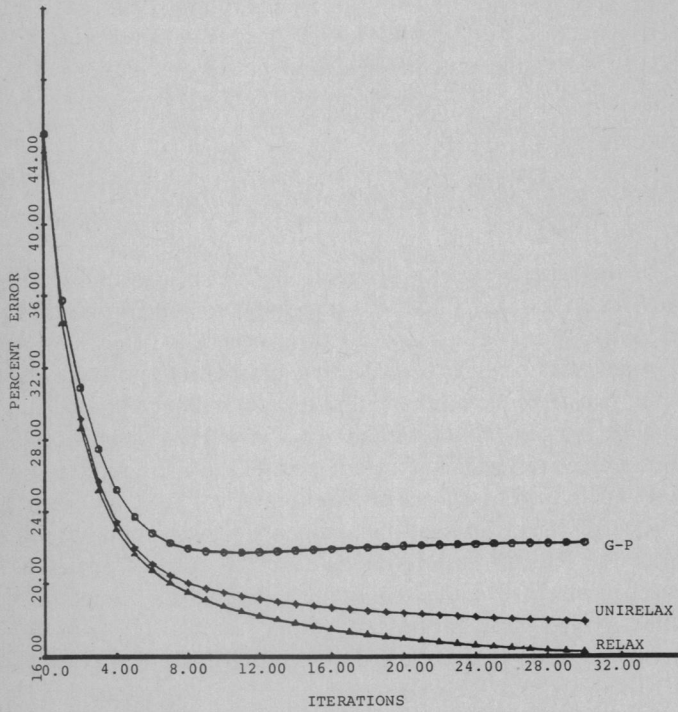


Fig. 8. Performance comparison of G-P, UNIRELAX, and RELAX in reconstructing from projection data available over $[-67^\circ, 67^\circ]$.

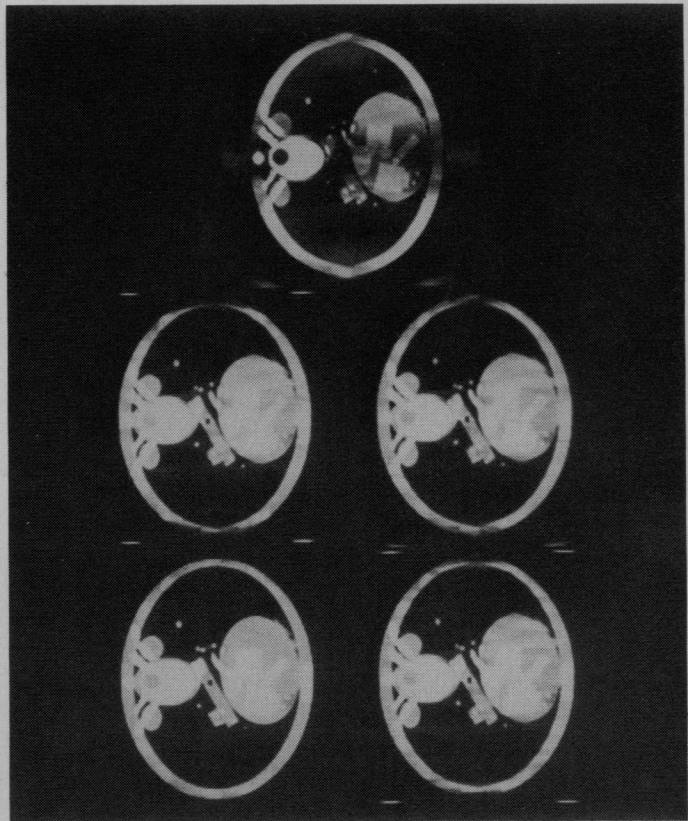


Fig. 9. Reconstructions when projection data are limited to $[-80^\circ, 80^\circ]$. Top: naive reconstruction; then clockwise from upper left: G-P, RELAX, UNIRELAX, and full view data reconstruction.

C. Results for When Projection Data Are Limited to $[-80^\circ, 80^\circ]$

The naive reconstruction ($e_o = 42$ percent) and the reconstructed images at the end of 30 iterations using RELAX, UNIRELAX, and G-P restorations are compared in Fig. 9. In Fig. 10 we compared the error performance of the reconstructions using RELAX, UNIRELAX, and G-P algorithms; the errors, are respectively 9.3, 12.1, and 15.5 percent at the end of 30 iterations. As before, reconstructions using *a priori* restoration is superior to the naive reconstruction. The reconstruction by the RELAX restoration outperforms the reconstruction performed by the classical G-P restoration. The G-P and RELAX reconstructions are compared to Fig. 11. The superior performance of RELAX is especially evident in reconstruction of the elliptical structure (note the obliterations in the G-P case) and the reduced plume-like clouding from the tips of bright objects.

VII. POTENTIAL APPLICATIONS IN NMR AND ULTRASOUND IMAGING

The PRDF algorithm is well-suited for applications where the frequency spectrum of the image function is directly measured or obtained from measurements. This can be the case in NMR and ultrasound (CAT) imaging.

In NMR imaging using LPR⁹ reconstruction [15] the Fourier

⁹LPR stands for line-integral projection reconstruction. In this technique, the gradient field is angularly varied and the NMR signal is recorded for a set of angular positions of the gradient field. This is analogous to collecting angular view data in X-ray CAT.

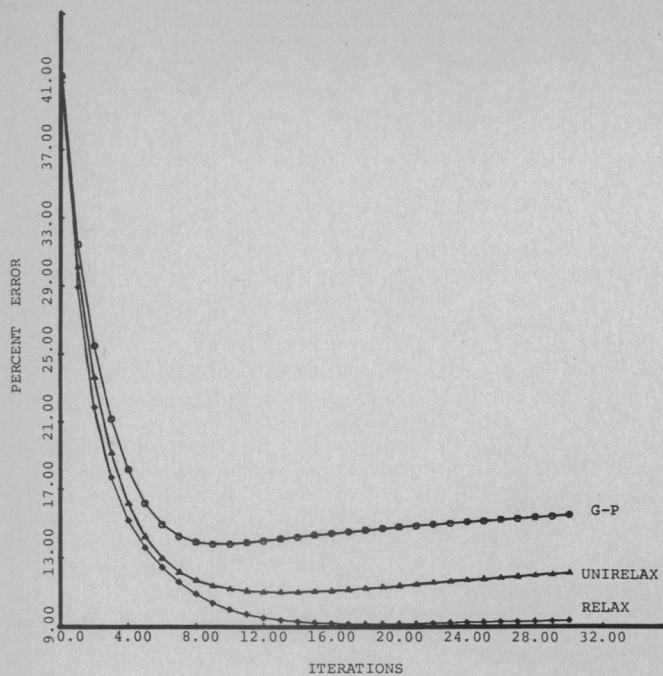


Fig. 10. Performance comparison of G-P, UNIRELAX, and RELAX in reconstructing from projection data available over $[-80^\circ, 80^\circ]$.

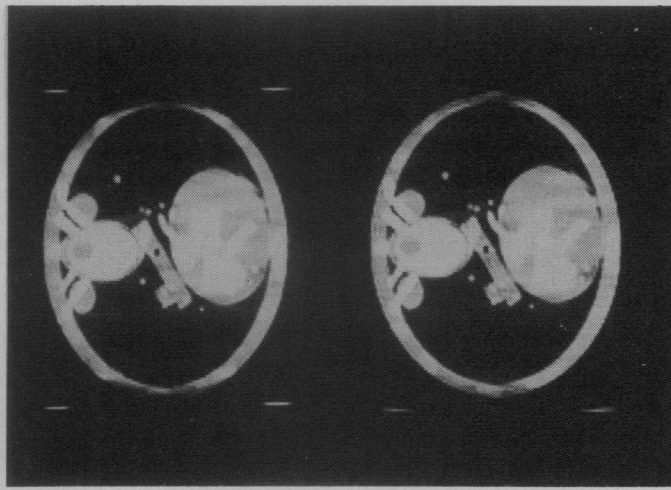


Fig. 11. G-P (left) and RELAX (right) reconstructions at 30th iteration.

transform of the image is obtained over a polar raster in the frequency domain [12], [15], [16], [17]. If complete spectrum information is available the direct Fourier inversion method (DFM) can be used to reconstruct the image. However, in the case of angularly view-limited measurements, the missing spectrum information can be restored via POCS prior to Fourier inversion. This restoration followed by Fourier inversion is indeed our PRDF reconstruction algorithm. *Angularly view-limited* measurements are motivated by the desire for reduction of data collection time.

In ultrasound computerized tomography (UCT) the spatial distribution of the real part of the refractive index, which involves the sonic velocity, and the imaginary part of the refractive index, which involves the attenuation coefficient, can be imaged. Neglecting diffraction effects, the line integrals, i.e., projection data of both sonic velocity and the

attenuation coefficient, can be estimated from measurements. However, if there are opaque obstructions such as bones or gas bubbles around the soft tissue of interest, the projection data for those views are useless and the viewing becomes essentially angularly limited. In this case the PRDF reconstruction is directly applicable.

When diffraction cannot be ignored such as in diffraction tomography, it may still be possible to use PRDF when the measured data are incomplete. Mueller *et al.* [18] considered diffraction tomography and solved the wave equation with certain assumptions. It is shown in [18] that the Fourier transform of the spatial refractive index distribution can be measured on circular arcs that pass through the origin of the frequency plane (see also [19] and [20]).

The data in the Fourier transform plane can be filled in by scanning the object with the insonifying source or by varying the frequency of the source. In UCT, the data are furnished along arcs in the frequency plane. In this form, it is difficult for the data to be processed by DFM. An important goal therefore is to develop a better interpolation technique than the *nearest neighbor* method presently used. Once this is done, it seems reasonable that PRDF can be used in diffraction tomography as well.

VIII. CONCLUSIONS AND SUMMARY

In this paper we presented a reconstruction algorithm (PRDF) that is synthesized from a recent restoration algorithm called projections onto convex sets (POCS) and from a direct Fourier inversion method (DFM) based on an exact polar-to-Cartesian interpolation formula. The PRDF algorithm is capable of performing reconstruction from angularly limited projection data. If the projection data are collected via fan beam geometry, rebinning [21] is applied prior to reconstruction to perform the conversion to equivalent parallel beam projection data. (Although missing view divergent data do not translate exactly into missing view parallel data.)

As noted before, DFM is a computationally faster algorithm than filtered convolution back-projection (FCBP). It is shown in [9] that DFM requires $O[N^2 \log N]$ operations compared with $O(N^3)$ operations for FCBP to reconstruct a similar quality ($N \times N$) image. However, one can use POCS with the FCBP algorithm as well to reconstruct from angularly limited projection data. Tuy [4] used POCS with the FCBP algorithm to solve the limited angular view problem.¹⁰ At the end of each iteration, the projection data over the missing angular range are generated for that iterate. This calculation can be time consuming and susceptible to numerical errors that may be introduced during the calculation.

We also discussed the possibility of applying the PRDF algorithm in NMR tomographic imaging and ultrasound computerized tomography. In NMR, unlike X-ray tomography, the frequency spectrum of the image distribution can be measured directly over a polar raster in the frequency domain. This fact suggests that NMR imaging is a potential candidate for the *interpolation and restoration* phase of the PRDF algorithm. In the case of ultrasound diffraction tomography the problem

¹⁰A similar algorithm is implemented on a commercial CAT scanner by Medoff *et al.* [22]. Choi *et al.* [23] proposed a similar algorithm to be used in ultrasound computerized tomography.

of interpolating over a Cartesian raster remains a future subject of investigation.

ACKNOWLEDGMENT

Many thanks are due to Dr. H. Tuy who supplied the thorax phantom data. We would also like to acknowledge our valuable technical discussions with him.

REFERENCES

- [1] D. C. Youla and H. Webb, "Image restoration by the method of convex projections: Part 1—Theory," *IEEE Trans. Med. Imaging*, vol. MI-1, pp. 81–94, Oct. 1982.
- [2] M. I. Sezan and H. Stark, "Image restoration by the method of convex projections: Part 2—Applications and numerical results," *IEEE Trans. Med. Imaging*, vol. MI-1, pp. 95–101, Oct. 1982.
- [3] A. Lent and H. Tuy, "An iterative method for the extrapolation of band limited functions," *J. Math. Anal. Appl.*, vol. 83, pp. 554–565, 1981.
- [4] H. K. Tuy, "An algorithm for incomplete range of views reconstruction," *Tech. Dig. Topical Meet. Signal Recovery, Synthesis with Incomplete Inform., Partial Constraints*, pp. FA1-1 and FA1-4, NV, Jan. 1983.
- [5] M. I. Sezan and H. Stark, "Image restoration by convex projections in the presence of noise," *Appl. Opt.*, vol. 22, pp. 2781–2789, Sept. 1983.
- [6] Z. Opial, "Weak convergence of the sequence of successive approximations for nonexpansive mappings," *Bull. Am. Math. Soc.*, vol. 73, pp. 591–597, 1967.
- [7] L. G. Gubin, B. T. Polyak, and E. V. Raik, "The method of projections for finding the common point of convex sets," *U.S.S.R. Comput. Math., Math. Phys.*, vol. 7, pp. 1–24, 1967.
- [8] A. Papoulis, "A new algorithm in spectral analysis and band-limited extrapolation," *IEEE Trans. Circuits, Syst.*, vol. CAS-22, pp. 735–742, 1975.
- [9] H. Stark, J. W. Woods, I. Paul, and R. Hingorani, "An investigation of computerized tomography by direct Fourier inversion and optimum interpolation," *IEEE Trans. Biomed. Eng.*, vol. BME-28, pp. 496–505, July 1981.
- [10] R. M. Lewitt, "Reconstruction algorithms: Transform methods," *Proc. IEEE*, vol. 71, pp. 390–408, Mar. 1983.
- [11] R. M. Mersereau and A. Oppenheim, "Digital reconstruction of multidimensional signals from their projections," *Proc. IEEE*, vol. 62, pp. 1319–1338, Oct. 1974.
- [12] Z. H. Cho *et al.*, "Direct Fourier reconstruction techniques in NMR tomography," in *Selected Topics, Image Science, Springer Verlag Lecture Notes in Medical Informatics*, vol. 23, 1984, to be published.
- [13] H. Stark, "Sampling theorems in polar coordinates," *J. Opt. Soc. Amer.*, vol. 69, pp. 1519–1525, Nov. 1979.
- [14] H. Stark and M. Wengrovitz, "Comments and corrections to 'the use of polar sampling theorems in CT,'" *IEEE Trans. Acoust., Speech, Signal Proc.*, vol. ASSP-31, pp. 1329–1331, Oct. 1983.
- [15] Z. H. Cho *et al.*, "Fourier transform nuclear magnetic resonance tomographic imaging," *Proc. IEEE*, vol. 70, pp. 1152–1173, Oct. 1982.
- [16] W. S. Hinshaw and A. H. Lent, "An introduction to NMR imaging: From the Bloch equations to the imaging equation," *Proc. IEEE*, vol. 71, pp. 338–350, Mar. 1983.
- [17] M. I. Sezan, "Image restoration by the method of projections onto convex sets with applications to tomographic image reconstruction from incomplete view data," Rensselaer Polytechnic Institute, Troy, NY, Ph.D. dissertation, May 1984.
- [18] R. K. Mueller, M. Kaveh, and G. Wade, "Reconstructive tomography and applications to ultrasonics," *Proc. IEEE*, vol. 67, pp. 567–587, Apr. 1979.
- [19] J. F. Greenleaf, "Computerized tomography with ultrasound," *Proc. IEEE*, vol. 71, pp. 330–337, Mar. 1983.
- [20] S. K. Kenue and J. F. Greenleaf, "Limited angle multifrequency diffraction tomography," *IEEE Trans. Sonics, Ultrasonics*, vol. SU-29, pp. 213–217, July 1982.
- [21] P. Dreike and D. P. Boyd, "Convolution reconstruction of fan beam projections," *Comput. Graphics, Image Process.*, pp. 459–469, 1976.
- [22] B. P. Medoff, W. R. Brody, M. Nassi, and A. Macovski, "Iterative convolution backprojection algorithms for image reconstruction from limited data," *J. Opt. Soc. Am.*, vol. 73, pp. 1493–1500, Nov. 1983.
- [23] J. S. Choi, K. Ogawa, M. Nakajima, and S. Yuta, "A reconstruction algorithm of body sections with opaque obstructions," *IEEE Trans. Sonics, Ultrasonics*, vol. SU-29, pp. 143–150, May 1982.
- [24] K. C. Tam and V. Perez-Mendes, "Tomographical imaging with limited angle input," *J. Opt. Soc. Am.*, vol. 71, pp. 582–592, 1981.